Journal of Computational Physics 229 (2010) 1626–1642

Contents lists available at ScienceDirect

Journal of Computational Physics

journal homepage: www.elsevier.com/locate/jcp

Generalized reference fields and source interpolation for the difference formulation of radiation transport ☆

Thomas Luu, Eugene D. Brooks III *, Abraham Szőke

Lawrence Livermore National Laboratory, P.O. Box 808, Livermore, CA 94550, USA

ARTICLE INFO

Article history:
Received 24 April 2009
Received in revised form 22 October 2009
Accepted 28 October 2009
Available online 6 November 2009

Keywords:
Difference formulation
Radiation transport
Implicit Monte Carlo

ABSTRACT

In the difference formulation for the transport of thermally emitted photons the photon intensity is defined relative to a reference field, the black body at the local material temperature. This choice of reference field combines the separate emission and absorption terms that nearly cancel, thereby removing the dominant cause of noise in the Monte Carlo solution of thick systems, but introduces time and space derivative source terms that cannot be determined until the end of the time step. The space derivative source term can also lead to noise induced crashes under certain conditions where the real physical photon intensity differs strongly from a black body at the local material temperature.

In this paper, we consider a difference formulation relative to the material temperature at the beginning of the time step, or in cases where an alternative temperature better describes the radiation field, that temperature. The result is a method where iterative solution of the material energy equation is efficient and noise induced crashes are avoided. We couple our generalized reference field scheme with an ad hoc interpolation of the space derivative source, resulting in an algorithm that produces the correct flux between zones as the physical system approaches the thick limit.

1. Introduction

The difference formulation for the transport of thermally emitted photons [1] was introduced to reduce the noise inherent in the Monte Carlo solution of the transport equation involving optically thick media. As the optical thickness of the material is increased the radiation field approaches that of a black body at the material temperature. In the Monte Carlo solution of a time dependent transport problem the change in the material energy during a time step is given by the difference between the stochastic absorption and the deterministic emission in a zone, providing a noisy solution as these two quantities approach each other. In the difference formulation, it is the difference between the photon field and a black body at the local material temperature that is transported via Monte Carlo, removing this source of noise [2].

When transforming from the radiation intensity field to the difference field, the thermal emission term is replaced with a time and space derivative source term while maintaining the same propagation and absorption behavior for the Monte Carlo particles. In problems where hot optically thin regions are surrounded by relatively cooler optically thick ones, such as the hohlraum environment for inertial confinement fusion, the space derivative source can become a source of cancellation induced noise. In this case, nearly equal weight particles of opposite sign cross the optically thin region and lead to fluctuations

☆ This work performed under the auspices of the US Department of Energy by Lawrence Livermore National Laboratory under Contract DE-AC52-07NA27344.

* Corresponding author. Tel.: +925 423 7341; fax: +925 423 8086.
E-mail address: brooks3@llnl.gov (E.D. Brooks).

0021-9991/$ - see front matter © 2009 Elsevier Inc. All rights reserved.
doi:10.1016/j.jcp.2009.10.049

in the energy absorbed on the surface of the enclosing optically thick region. In the most severe situations these fluctuations lead to problem crashes.

A piecewise-constant treatment of source terms, constant within a zone, is often used in Monte Carlo simulations of the transport equation. That this leads to excessive equilibrium energy flow is easy to see in the difference formulation, where the source term that survives in the equilibrium limit is the space derivative source. A piecewise-constant treatment of the space derivative source concentrates this source at the interface between zones, causing it to contribute to the energy flow between zones in its entirety, leading to excessive energy flow. A self-consistent linear finite element treatment [3,4] addresses excess energy flow, but can be complicated to implement in two and three dimensional geometries. Although self-consistent finite element methods resolve the excess energy flow problem, a simpler treatment of the source terms that would provide correct energy flow in the thick limit will enable easier application of the Monte Carlo method in practice.

Stable time dependent solution of transport problems via the Monte Carlo method have required implicit treatment of the source term strengths. Satisfying this requirement led to effective scattering in the Implicit Monte Carlo (IMC) [5] method, and has also led to matrix energy deposition in the Symbolic Implicit Monte Carlo (SIMC) [6] method. The IMC method stabilizes the time evolution by reducing the coupling between the radiation field and the material [7,8]. In the SIMC method the coupling remains physical, but at the cost of a non-linear system solve that scales poorly as the number of zones in the problem is increased. This becomes a concern for large problems in two and three dimensions.

In the difference formulation, we are free to choose a black body corresponding to a temperature other than the local material temperature for the reference field without introducing any approximation. In this paper, we show how one can exploit this freedom to limit the space derivative source term at an interface between thick and thin regions where it might increase Monte Carlo noise, alleviating the problem crashes that can occur when these sources border optically thin regions. Additionally, the freedom to choose the reference field can be used to remove the unknown end of time step temperatures from the time and space derivative source terms that appear in the difference formulation. By doing this, we simplify the sampling of these source terms and remove matrix scoring for the associated particles as their weights are known. The cost of our adjustment to the reference field is that the thermal emission source term is not completely cancelled. A remainder source term, unknown until the end of the time step, arises from the change in the material temperature during the time step. For slowly varying problems, the remainder source term is small and leads, quite naturally, to an iterative method for the solution of the end of time step temperatures.

This paper is organized in the following manner: In Section 2 we review the difference formulation and describe in some detail the motivation for choosing the reference field more generally than we have done in the past. Section 3 then explains our discretization scheme and describes our method of solving the equation for the material energy. Here we present an ad hoc interpolation of the space derivative source which removes the excessive energy-flow associated with a piecewise-constant treatment of the material temperature. We also show that choosing a black body corresponding to the material temperature at the beginning of the time step for the reference field leads to an iterative method for the solution of the material energy equation. In Section 4 we show how to suitably modify the choice of reference field in problems including both optically thin and optically thick regions so that noise induced problem crashes are avoided. In Section 5 we provide a synopsis of a stability analysis we have performed for the generalized reference field approach, the details of which can be found in [9]. We conclude in Section 6.

2. The difference formulation with a generalized reference field

Radiation transport in media is described by the Boltzmann equation for photons coupled to the material energy equation, which in slab geometry under the assumptions of no scattering, no material motion, and local thermodynamic equilibrium (LTE) for the material is given by

$$\left(\frac{1}{c}\frac{\partial}{\partial t}+\mu\frac{\partial}{\partial x}+\sigma\right)I=\sigma B, \tag{1}$$

$$\frac{\partial E}{\partial t}=2\pi\int dv\,d\mu\sigma(I-B)+G. \tag{2}$$

The change in the energy density of the material, E, is related to the change in its temperature, T, by its density, ρ, times the specific heat, c_v, which may itself be a function of temperature,

$$dE=\rho c_v\,dT. \tag{3}$$

Here I represents the intensity field for photons, $1/\sigma$ their absorption length, v their frequency, μ the direction cosine of photon travel, B the blackbody field at the material temperature given by

$$B=\frac{2hv^3}{c^2}\frac{1}{e^{hv/kT}-1}, \tag{4}$$

and G is a local heating rate for the material. The black body emission function, Eq. (4), can be expressed in terms of a "reduced" frequency distribution function, $b(v,T)$,

$$B(v,T)=\frac{caT^4}{4\pi}b(v,T), \tag{5}$$

where a is the radiation constant. The advantages of using the reduced frequency distribution function are that the strong temperature dependence of thermal emission is factored out by the T^4 term, and that its frequency integral is independent of temperature,

$$\int_0^\infty dv b(v,T) = 1. \tag{6}$$

There is an extensive collection of numerical algorithms that have been developed for solving the coupled equations above after discretization in space and time (see [10] and references within for a review of existing algorithms). These algorithms use implicit discretization in time for numerical stability.

The difference formulation employed in [1,2,4,11] defined the difference field as $D = I - B$, where B is the black-body radiation field at the material temperature at each point in space and time, with the exception of special treatment of boundary conditions that reduced Monte Carlo noise. In terms of the difference field, D, Eqs. (1) and (2) become

$$\left(\frac{1}{c}\frac{\partial}{\partial t} + \mu\frac{\partial}{\partial x} + \sigma\right)D = -\left(\frac{1}{c}\frac{\partial}{\partial t} + \mu\frac{\partial}{\partial x}\right)B, \tag{7}$$

$$\frac{\partial E}{\partial t} = 2\pi\int dv\, d\mu \sigma D + G. \tag{8}$$

Note that in this formulation, the original σB source of Eq. (1) is replaced by the derivative sources

$$-\left(\frac{1}{c}\frac{\partial}{\partial t} + \mu\frac{\partial}{\partial x}\right)B. \tag{9}$$

The vices and virtues of this particular transformation are discussed in detail in [1,2].

The difference formulation is not restricted to using the black body field corresponding to the local material temperature, B, as the reference field. Any choice for the reference field, $\overline{B}$, may be used and the resulting formulation of the transport equation will still be rigorously equivalent to the original one. If the black body corresponding to the material temperature is used, the Monte Carlo noise arising from the near cancellation of thermal emission and absorption, $\sigma(I - B)$ in Eq. (2), that occurs in optically thick regions is removed. When the actual intensity, I, is very different from B, as might occur in optically thin regions where radiation flows freely, alternative choices for the reference field are advantageous. They reduce other sources of noise in a Monte Carlo implementation of the transport algorithm.

We now generalize the difference formulation by defining $D = I - \overline{B}$ where $\overline{B}$ is the black body function given by Eq. (4) at some judiciously chosen temperature, $\overline{T}$.[1] In this case the transport and energy equations become

$$\left(\frac{1}{c}\frac{\partial}{\partial t} + \mu\frac{\partial}{\partial x} + \sigma\right)D = \sigma(B - \overline{B}) - \left(\frac{1}{c}\frac{\partial}{\partial t} + \mu\frac{\partial}{\partial x}\right)\overline{B}, \tag{10}$$

$$\frac{\partial E}{\partial t} = 2\pi\int dv\, d\mu \sigma D - 2\pi\int dv\, d\mu\ \sigma(B - \overline{B}) + G. \tag{11}$$

Obviously, if $\overline{B} = B$ one recovers Eqs. (7) and (8). When $\overline{B} = 0$, one recovers Eqs. (1) and (2).

There are several motivations for using a generalization of the difference formulation. If $\overline{B}$ is known at the beginning of the time step, the derivative sources in Eq. (10),

$$-\left(\frac{1}{c}\frac{\partial}{\partial t} + \mu\frac{\partial}{\partial x}\right)\overline{B}, \tag{12}$$

are themselves known. This makes these sources easier to sample in complicated geometries, reduces the cost of scoring the particles, and reduces the complexity of the nonlinear system that represents the energy equation. In this case, the only source that contains unknown factors is the remainder source

$$\sigma(B - \overline{B}), \tag{13}$$

which, aside from any complicated frequency dependence of σ, is relatively simple to sample as it is isotropic. If $\overline{B}$ is the value of B at the beginning of the time step and the problem is slowly varying, the unknown remainder source term, $\sigma(B - \overline{B})$, is small and can be handled as a perturbation on the otherwise explicit solution for the transport equation, making it amenable to iterative solution techniques. In particular, we have found an iterative solution strategy that directly addresses the nonlinear problem without requiring the solution of a linear system within each step of a Newton–Raphson iteration.

Another, perhaps more important, motivation for a generalized difference formulation comes from the fact that there can be regions of a problem where the radiation temperature that corresponds to the radiation energy density is not close to the material temperature. If the radiation and the material temperatures differ by a significant amount, a Monte Carlo solution of Eqs. (7) and (8) will be intrinsically noisy due to the large difference field, and this can be aggravated (to the point of a code crash) by the fact that the difference field is a signed quantity. Such a scenario can occur, for example, in problems that have both optically thick and thin regions with significantly different material temperatures. Because of weak coupling between the radiation and material in the optically thin regions, the radiation temperature in these regions is dominated by the

[1] One is not limited to defining the reference field, $\overline{B}$, in terms of a blackbody at some temperature, see for example the P_1 scheme in [12].

material temperature in the adjacent optically thick regions. Thus, within the optically thin regions, a choice for $\overline{B}$ that tracks the material temperature of the adjacent optically thick regions produces a small difference field, D, and therefore lowers Monte Carlo noise. The utility of this modification to the reference field is demonstrated in the results shown in Section 4.3.

3. Discretization scheme and Monte Carlo energy weights

In order to solve the time dependent transport problem posed in Eqs. (10) and (11), with suitable boundary conditions, the problem domain is divided into N zones, enumerated by $1 \leqslant i < N$ with the left edge of the zone at x_i and its right edge at x_{i+1}. Except for the possibility of interpolating the space derivative source between zone centers, the treatment of the material state variable and the reference field is constant within a zone, during a time step. The transport equation is "solved" by working out the total energy of the source terms and emitting it as Monte Carlo particles with appropriate coordinate distributions. Each Monte Carlo particle carries an energy weight that decays exponentially as it travels, losing energy to the material. The change in the material energy for the time step, from t_0 to $t_0 + \Delta t$, is accounted for in each zone by evaluating the integrals in Eq. (11) over the time step. These integrals are evaluated by scoring Monte Carlo particles, track by track, along with deterministic integrals that arise due to the possibility that the reference field, $\overline{B}$, may not cause complete cancellation of the thermal emission term, σB.

The Monte Carlo particles that are tracked through the time step, t_0 to $t_0 + \Delta t$, are composed of the census particles from the prior time step, particles that are born during the time step due to the source terms given by Eqs. (12) and (13), and any particles that arise from the boundary conditions for the problem. As has become well known for implicit Monte Carlo transport of thermally generated photons, we need to use the unknown end of time step value for B in our source terms if we are to obtain stable time dependent behavior.

The requirement for implicit treatment of B leads to Monte Carlo particles with energy weights that will not be known until the end of the time step. The Symbolic Implicit Monte Carlo method [6] is used to account for the energy deposition from these particles. The energy equation, Eq. (11), becomes a nonlinear matrix equation in this scheme. Its solution provides the material energy, or equivalently, the material temperature, at the end of the time step. By exploiting the freedom we have in the choice for $\overline{B}$, we minimize the costs associated with the SIMC method while maintaining an unconditionally stable solution.

3.1. Monte Carlo sources

We begin by noting that the frequency dependence of the sources can be factored out in the following manner,

$$\left(\frac{1}{c}\frac{\partial}{\partial t} + \mu\frac{\partial}{\partial x}\right)\overline{B} = \frac{4\pi}{c}\frac{\partial \overline{B}}{\partial \overline{\Phi}}\left(\frac{1}{4\pi}\frac{\partial \overline{\Phi}}{\partial t} + \frac{\mu c}{4\pi}\frac{\partial \overline{\Phi}}{\partial x}\right). \tag{14}$$

Here $\overline{\Phi}(t) = a\overline{T}^4(t)$ is a constant during the time step, $(t_0 \leqslant t < t_0 + \Delta t)$, and $\partial\overline{B}/\partial\overline{\Phi}$ represents a frequency distribution since it is positive and satisfies

$$\frac{4\pi}{c}\int_0^\infty dv \frac{\partial \overline{B}}{\partial \overline{\Phi}} = 1. \tag{15}$$

Efficient techniques have been developed for sampling the integrand in Eq. (15) [4].

3.1.1. Time derivative source $-\partial\overline{B}/c\partial t$

As $\overline{B}$ is constant within a zone, abruptly jumping in value at the beginning of each time step, the Monte Carlo particles associated with the time derivative source term are emitted at the beginning of each time step. They are uniformly emitted in μ and across the zone of width $\Delta x = x_{i+1} - x_i$ with a total weight given by

$$-\frac{\Delta x}{2\pi}[\overline{\Phi}_i(t_0 + \varepsilon) - \overline{\Phi}_i(t_0 - \varepsilon)], \tag{16}$$

where ε is a small interval in time to make it clear that we are referring to values before and after the jump at the beginning of the time step. The weights of these particles may be known, or not, depending upon the choice we make for the reference field.

3.1.2. Space derivative source $-\mu\partial\overline{B}/\partial x$

If $\overline{B}$ is constant within each zone, the Monte Carlo particles associated with the space derivative source term are emitted at the edge of each zone. The factor of μ in this source term introduces a signed direction dependence that we handle with correlated particle pairs, sampling positive μ and then emitting a correlated particle in the $-\mu$ direction with the opposite weight. The strength of the positive μ portion of this source at the zone edge x_i, discussed in [2], is

$$-\Delta t\frac{c}{8\pi}(\overline{\Phi}_i - \overline{\Phi}_{i-1}), \tag{17}$$

where $\overline{\Phi}_i$ is the value of $\overline{\Phi}$ in zone i during the time step. The weights of these particles may be known, or not, depending upon the choice we make for $\overline{B}$.

3.1.3. Interpolation of space derivative sources $-\mu\partial\overline{B}/\partial x$

The piecewise-constant spatial discretization for $\overline{B}$ leads to excessive energy flow in the thick limit [4,11] because the source is concentrated at the zone edge where all of its strength contributes to energy flow between the zones. To alleviate excess energy flow, we construct our space derivative sources by linearly interpolating zone centered material state variables. In this manner, we work with *shifted*, or *dual* zones. The left edge of an interior *dual* zone $j \in (2, N)$ is $(x_{j-1} + x_j)/2$ and the right edge is $(x_j + x_{j+1})/2$. The interpolated field for interior dual zone j is given by

$$\widetilde{\Phi}_j(x,t) = \left[\frac{x_{j+1} + x_j - 2x}{x_{j+1} - x_{j-1}}\right]\overline{\Phi}_{j-1}(t) + \left[\frac{2x - x_j - x_{j-1}}{x_{j+1} - x_{j-1}}\right]\overline{\Phi}_j(t), \tag{18}$$

while the interpolated field for the half zones at the problem boundaries, $\widetilde{\Phi}_1(x,t)$ and $\widetilde{\Phi}_{N+1}(x,t)$, (or equivalently, zone interfaces between significant changes in material properties) are given by straight line extrapolation from $\widetilde{\Phi}_2(x,t)$ and $\widetilde{\Phi}_N(x,t)$, respectively.

We construct our space derivative sources using the interpolated field defined by Eq. (18) and the extrapolations for the half zones at problem boundaries. The source within each interior dual zone j is then given by

$$-\frac{\mu c}{4\pi}\frac{\partial\widetilde{\Phi}_j(x,t)}{\partial x} = \frac{\mu c}{2\pi}\left[\frac{\overline{\Phi}_j(t) - \overline{\Phi}_{j-1}(t)}{x_{j+1} - x_{j-1}}\right], \tag{19}$$

remembering that the index j of $\widetilde{\Phi}_j$ refers to the dual zone j, while the indices on the right hand side of the equation refer to zone indices of the original piecewise-constant discretization. Monte Carlo sampling of this source term is done with a uniform distribution within the dual zone (as opposed to delta functions at the zone edges).

Spreading out the space derivative source term in this manner produces the correct flux between zones as one approaches equilibrium in the thick limit. In the case that the opacity of the two adjoining zones is not identical, we can either use a "kinked" interpolation that conserves the diffusion limit flux across the interface, or we can use extrapolation of the slope from the next dual zone if the opacity does not change. The best thing to do depends on the dynamic conditions and the severity of the change in opacity. A more accurate treatment would use the full machinery of the linear discontinuous finite element method [4]. The goal of this interpolation method is to reduce cost, compared to the finite element method, for implementations in higher dimensions. We interpolate only the space derivative source.

3.2. Two examples of $\overline{B}$

3.2.1. End of time step reference field

Our first example of a reference field is the 'end of time step' (implicit) field

$$\overline{B}(t) = B(t_0 + \Delta t) \quad (t_0 \leqslant t < t_0 + \Delta t), \tag{20}$$

the same reference field used in [11,4]. Monte Carlo transport of particles is governed by Eqs. (7) and (8) with the weights defined in the above sections. In this case, there are no remainder sources and the material opacity enters only during absorption.

3.2.2. Beginning of time step reference field

Our second example of a reference field is the 'beginning of time step' (explicit) field

$$\overline{B}(t) = B(t_0) \quad (t_0 \leqslant t < t_0 + \Delta t). \tag{21}$$

Here $\overline{B}$ is a series of step functions in time; its value for the duration of the time step, from t_0 to $t_0 + \Delta t$, being the known value of B determined at the end of the prior time step. The source terms, given by Eq. (12), are known, and do not contribute to off-diagonal terms in the nonlinear system that must be solved in order to resolve the change in material energy at the end of the time step.

The remainder source in zone i, during the time interval from t_0 to $t_0 + \Delta t$, is given by

$$\sigma(B_i - \overline{B}_i) = \sigma\frac{4\pi}{c}\frac{\partial B}{\partial \Phi}\left[\frac{c}{4\pi}(\Phi_i(t_0 + \Delta t) - \Phi_i(t_0))\right], \tag{22}$$

where we are assuming small changes in Φ. (There are situations, such as the reference field choice of Section 4.3.3, where the difference in Φ for the remainder source term is large. These require the use of a finite difference approach for the construction of the frequency distribution.) Integrating this within zone i, across the time step from t_0 to $t_0 + \Delta t$, over the range of direction cosines, and over all frequencies, the total energy weight associated with this source is given by

$$\int_{x_i}^{x_{i+1}} dx \int_{t_0}^{t_0+\Delta t} dt \int_{-1}^{1} d\mu \int d\nu \sigma(B_i - \overline{B}_i) = \frac{c\Delta x\Delta t}{2\pi}\langle\sigma\rangle_i[\Phi_i(t_0 + \Delta t) - \Phi_i(t_0)], \tag{23}$$

where

$$\langle\sigma\rangle_i = \frac{4\pi}{c}\int dv\ \sigma\frac{\partial\overline{B}_i}{\partial\overline{\Phi}_i}. \tag{24}$$

The frequency distribution of this source is given by

$$\frac{4\pi}{c}\sigma\frac{\partial\overline{B}_i}{\partial\overline{\Phi}_i}/\langle\sigma\rangle_i. \tag{25}$$

For gray opacities $\langle\sigma\rangle_i = \sigma$.

3.3. Newton–Raphson solution strategy for finding the material energy E

The unknowns, $\Phi_i(t_0+\Delta t)$, are calculated by solving the material energy equation, Eq. (11), at the end of the time step, $t_0+\Delta t$. To accomplish this, we first formally integrate Eq. (11) from t_0 to $t_0+\Delta t$ to obtain the following function,

$$\begin{aligned} f(x) = {} & E(T(x,t_0)) - E(T(x,t_0+\Delta t)) + 2\pi\int_{t_0}^{t_0+\Delta t} dt\int dv\int d\mu\sigma(v,T(x,t_0))D(x,t;v,\mu) + \int_{t_0}^{t_0+\Delta t} dt\ G(x,t) \\ & - 2\pi\int_{t_0}^{t_0+\Delta t} dt\int dv\int d\mu\sigma(B-\overline{B}). \end{aligned} \tag{26}$$

We then integrate $f(x)$ within each zone i, thereby defining the following quantities,

$$\begin{aligned} f_i &= \int_{x_i}^{x_{i+1}} dx f(x), \\ &= E_i(t_0) - E_i(t_0+\Delta t) + (\sigma D)_i + G_i - (\sigma\Delta B)_i, \end{aligned} \tag{27}$$

where

$$E_i = \int_{x_i}^{x_{i+1}} dx E(T) = \Delta x_i\frac{\rho c_v}{a^{1/4}}\ \Phi_i^{1/4}, \tag{28}$$

$$G_i = \int_{x_i}^{x_{i+1}} dx G(x), \tag{29}$$

$$\begin{aligned} (\sigma\Delta B)_i &= 2\pi\int_{x_i}^{x_{i+1}} dx\int_{t_0}^{t_0+\Delta t} dt\int dv\int d\mu\sigma(B-\overline{B}) \\ &= c\langle\sigma\rangle_i\Delta x\ \Delta t[\Phi_i(t_0+\Delta t) - \overline{\Phi}_i(t_0)], \end{aligned} \tag{30}$$

and

$$\begin{aligned} (\sigma D)_i &= 2\pi\int_{x_i}^{x_{i+1}} dx\int_{t_0}^{t_0+\Delta t} dt\int dv\int d\mu\sigma(v,T(x,t_0))D(x,t;v,\mu) \\ &= N_i + \sum_j (REM)_i^j(\Phi_j(t_0+\Delta t) - \overline{\Phi}_j(t_0)) + \sum_j (DDT)_i^j\ (\overline{\Phi}_j(t_0) - \overline{\Phi}_j(t_0-\Delta t)) + \sum_j (DDX)_i^j\ (\overline{\Phi}_{j-1}(t_0) - \overline{\Phi}_j(t_0)). \end{aligned} \tag{31}$$

We have assumed that ρC_v is constant within each zone, during the time step. N_i is the contribution from the census particles to zone i from the prior time step, $(REM)_i^j$ is the contribution to zone i due to remainder sources, $\sigma(B_j-\overline{B}_j)$, emanating from zone j, $(DDT)_i^j$ is the contribution to zone i from the time derivative sources emanating from zone j, and $(DDX)_i^j$ is the contribution to zone i from space derivative sources from edge j. Note the nonlinearity of Φ in Eq. (28). Our unknown $\Phi_j(t_0+\Delta t)$ are found by demanding that $f_i = 0$ for all i. We solve for these by way of a Newton–Raphson iteration algorithm.

We note that if $\overline{\Phi}_j = \Phi_j(t_0)$, only the portion of $(\sigma D)_i$ due to remainder sources in Eq. (27) carry a dependence on the unknown $\Phi_j(t_0+\Delta t)$ for spatial zones $j\neq i$, while if $\overline{\Phi}_j = \Phi_j(t_0+\Delta t)$ the difference formulation introduced in [1] is recovered.

3.4. Alternative iterative solution strategy for finding the material energy

The Newton–Raphson procedure described above converges quickly but requires the solution of a linear system for the error at each step. The cost of solving the linear system scales poorly as the number of zones in the problem is increased. In order to address this problem, we have developed an alternative iterative solution strategy that is a variant of Jacobi iteration. We provide a synopsis of Jacobi iteration here and then show how to solve the nonlinear material energy equation using a similar strategy.

Assuming that one wants the solution to

$$Ax = b, \tag{32}$$

one decomposes the matrix A into $A = D + L + U$, where D is a diagonal matrix, L is lower triangular and U is upper triangular. Rewriting, one obtains

$$Dx = [b - (L+U)x]. \tag{33}$$

If all of the diagonal matrix elements are nonzero, Eq. (33) can be used as a prescription for iterating a solution for x,

$$x^{k+1} = D^{-1}[b - (L+U)x^k]. \tag{34}$$

If the original matrix, A, is diagonally dominant this iterative process, known as Jacobi iteration, converges.

Examining Eq. (27)–(31), we see that Eq. (27) can be put in the form

$$NL(x^{1/4}) + Ax = b, \tag{35}$$

where x is a vector of the unknowns, $\Phi_j(t_0+\Delta t), (x^{1/4})$ is a vector of $\Phi_j^{1/4}(t_0+\Delta t), NL$ is a diagonal matrix and A can be decomposed into $A = D + L + U$. Rewriting, and casting into a form similar to the case for Jacobi iteration, we obtain

$$NL(x^{1/4})^{k+1} + Dx^{k+1} = b - (L+U)x^k. \tag{36}$$

The left hand side is not a linear operator, so the refined solution is not obtained by simple division. A particular root of a quartic equation, however, produces each element of x^{k+1}.

At the cost of a reduced rate of convergence, compared to Newton–Raphson iteration, the solution of a linear system has been traded for a matrix-vector multiply. The method can be extended to handle real material specific heats that are functions of temperature. One could also explore the effectiveness of Newton–Raphson iteration using an iterative linear solver at its core, that might provide faster convergence than this nonlinear extension of Jacobi iteration.

4. Computational results

4.1. Removal of excessive energy flow for optically thick zones

We now show comparisons of runs with and without interpolation of space derivative sources, demonstrating that interpolation removes excess energy flow. Fig. 1 shows comparisons of a calculated Marshak wave at $t = 30$ sh (1 sh (shake) $= 1 \times 10^{-8}$ s) using our interpolation scheme and the original piecewise-constant treatment, for: (a) 12.5, (b) 25, (c) 50, and (d) 100 mean free paths (mfp) per zone. The initial temperature of the slab was zero, the left boundary at 0 cm is in contact with a heat bath held at 1 keV, the right boundary at 5 cm is open to vacuum, the heat capacity is $c_v = .1$ jerk/cm keV (1 jerk $= 10^9$ J) and opacity of the material is $\sigma = 200/\text{cm}$. In each of the four panels of the figure, the black lines represent the piecewise-constant calculations while the red lines are calculated using interpolation of the space derivative source.

For the piecewise constant discretization, the temperature profile of the Marshak wave changes as the optical thickness of the zone changes and the results have not really begun to converge. Convergence would require zones less than one mean free path thick. The solution using our interpolation method is well converged and agrees well with the linear finite element method [4].

We also calculate Larsen's test problem as originally defined in [14]. Here a slab with thickness of 4 cm is heated by a 1 keV radiative source at the *right* boundary. The heat capacity of the slab is constant, .05109 jerk/cm^3 keV. The opacity is defined as

$$\sigma(v,T,x) = \sigma_o(x)\frac{1 - e^{-hv/kT}}{(hv/\text{keV})^3},$$

where

$$\sigma_o(x) = \begin{cases} 1\ \text{keV}^3/\text{cm}, & 0 < x < 1, \\ 1000\ \text{keV}^3/\text{cm}, & 1 < x < 2, \\ 1\ \text{keV}^3/\text{cm}, & 2 < x < 4. \end{cases}$$

This opacity closely models inverse Bremsstrahlung absorption corrected for stimulated emission. We do not enforce continuity in the interpolated fields $\tilde{\Phi}$ at locations where discontinuities in opacity occur. The spatial zoning is also defined as

$$\Delta x = \begin{cases} .10\ \text{cm}, & 0 < x < 1, \\ .02\ \text{cm}, & 1 < x < 2, \\ .20\ \text{cm}, & 2 < \text{x} < 4. \end{cases}$$

As there is no analytic solution, we compare our result with a similar calculation done using a much finer spatial zoning as seen in Fig. 2. The plots show results at a time $t = .090$ sh, or 900 ps, using a time step of .001 sh (10 ps). We also compare to calculations using the piecewise-constant algorithm (no interpolation) in Fig. 3. Panel (a) of this figure shows a close-up of the interior optically thick region with calculations using interpolation and zone refinements of $1\times$, $2\times$, $4\times$, and $8\times$ the original zoning. Panel (b) shows the analogous results using the piecewise-constant algorithm. Note the slight excess energy flow in this latter case, and the slower convergence with zone size refinement. We note that sampling of the frequency in these calculations was easy due to the fact that σ does not appear in the time and space derivative source terms, although it does appear in the remainder source term if it is present. Our results agree very well with those shown in [15].

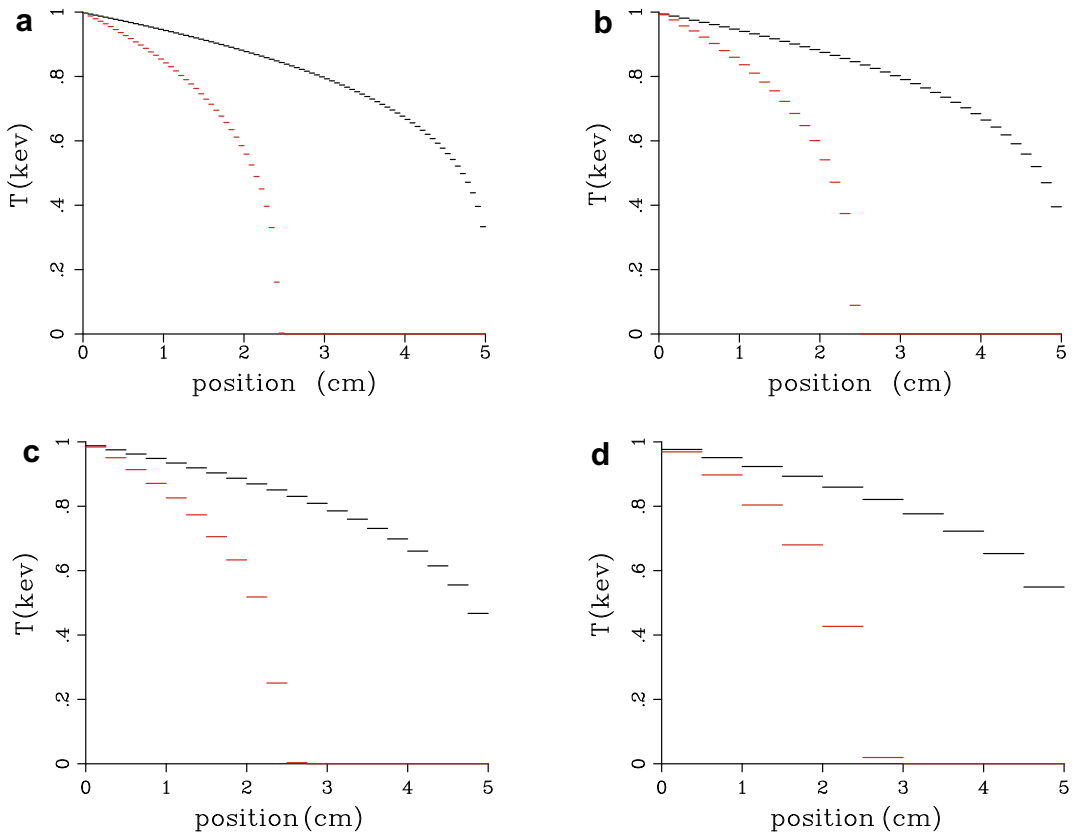

Fig. 1. Comparison of interpolation (see Section 3.1.3) versus original piecewise-constant treatment for a 1 keV driven Marshak wave at $t = 30$ sh with initial slab temperature being zero. Panel (a) represents a calculation using 12.5 mfp/zones, (b) 25 mfp/zones, (c) 50 mfp/zones, and (d) 100 mfp/zones. In each panel, the result shown in black is the piecewise-constant treatment, while the result shown in red uses interpolation.

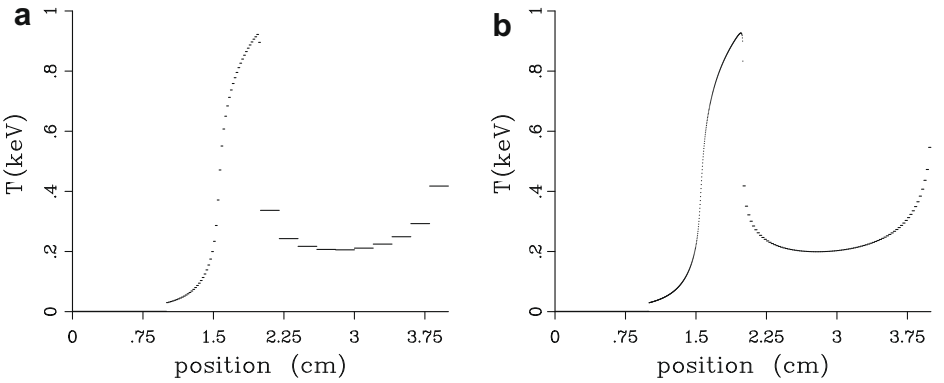

Fig. 2. Plot (a) shows the result of Larsen's test problem at total time $t = .09$ sh using $\Delta t = .001$ sh and spatial zoning as defined in the text. Plot (b) shows the same calculation but with spatial zoning that is eight times finer.

4.2. Alternative iterative solver

We now give an example of the efficacy of using a reference field $\overline{B}$ defined in Eq. (21) in combination with our alternative iterative solver described in Section 3.4. When using the alternative iterative solution strategy, at each time step the iteration is ended when our prescribed figure of merit,

$$\varepsilon = \sqrt{\sum_i \left(\frac{\Phi_i^{k+1} - \Phi_i^k}{\Phi_i^k} \right)^2}, \tag{37}$$

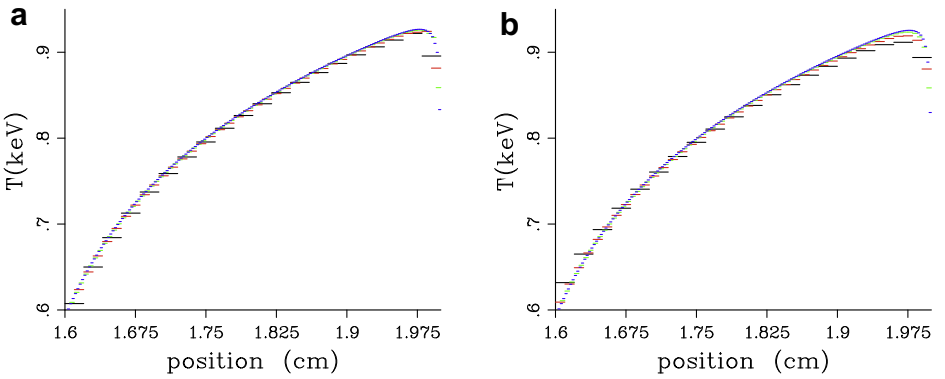

Fig. 3. Plot (a) shows a close up of Larsen's test problem at $t = .09$ sh using our interpolation algorithm with $1\times$, $2\times$, $4\times$, and $8\times$ the original zoning. Plot (b) shows similar results, but without source interpolation. Note the excess energy flow and the stronger dependence on zone sizes in the latter case.

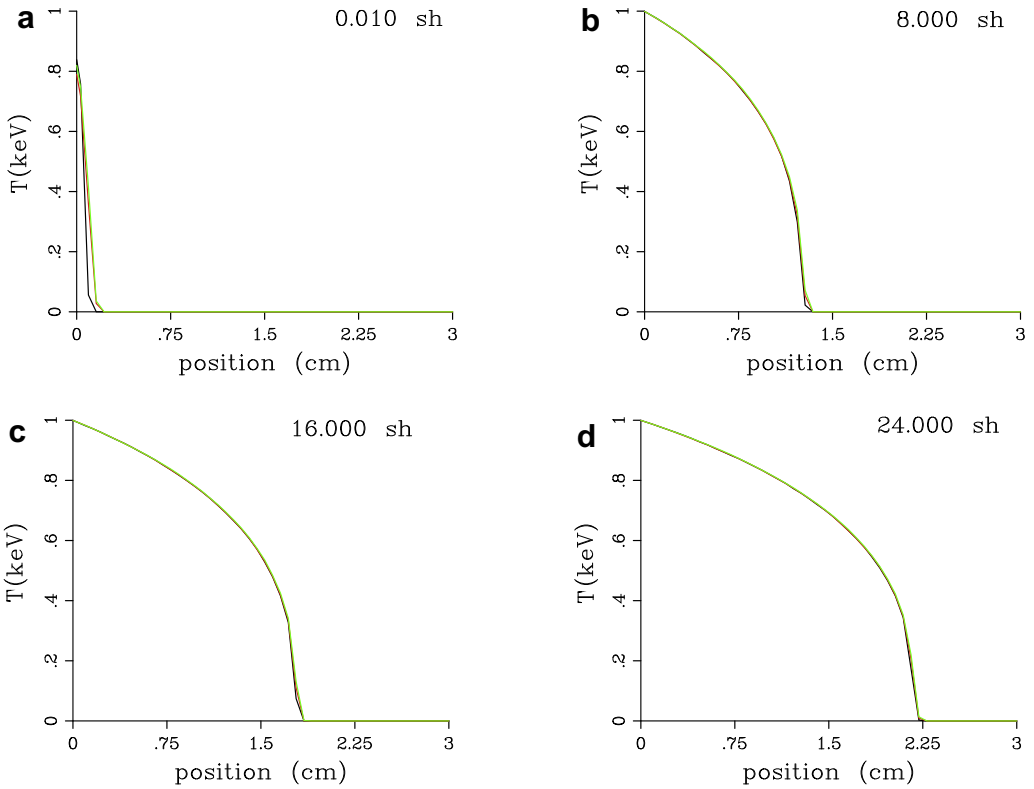

Fig. 4. Comparison of Marshak wave calculations at various times using $\overline{B} = B(t_0)$ with the Newton–Raphson solution strategy (red) and alternative iterative solution strategy (green) described in text. Also shown are results of the original difference formulation, using $\overline{B} = B(t_0 + \Delta t)$ (black).

is less than some pre-defined value. Here the sum is over all zones, i, and the superscripts $k+1$ and k refer to the iteration step given by Eq. (36).

Here we run Marshak wave calculations using a gray $\sigma = 200\ \text{cm}^{-1}$, $\rho C_v = .1$ jerk/cm^3, and 80 equally spaced zones over a slab of length 5 cm, giving 12.5 mean free paths per zone. A time step size of 0.01 sh is used in these calculations. The temperature at the left edge of the problem is held at 1 keV and the temperature of the slab is initially zero. Fig. 4 shows our results at various times, where we have performed our calculations using both the Newton–Raphson solution strategy (red)[2] and alternative iterative solution strategy (green) described in the previous section. Our termination criterion for these

[2] For interpretation of color in Figs. 4, 6, 7, and 11, the reader is referred to the web version of this article.

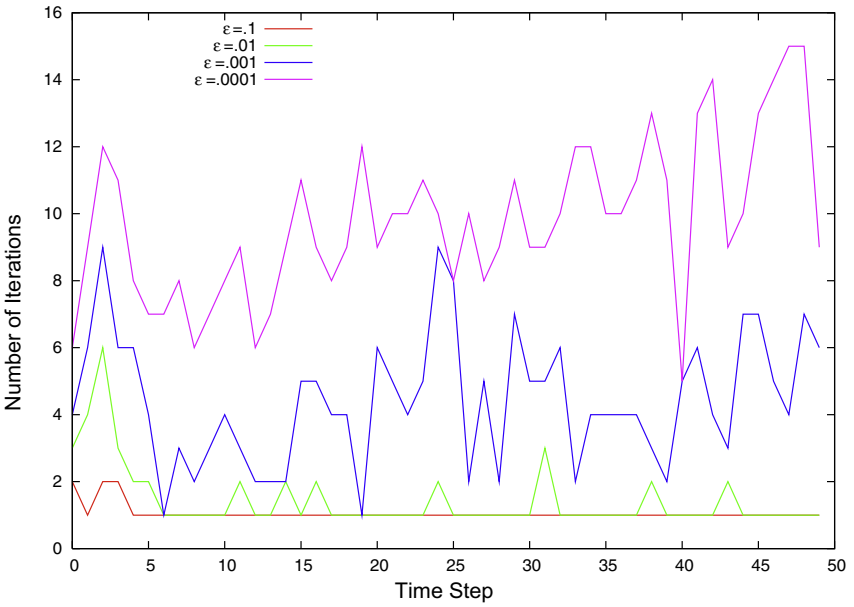

Fig. 5. Number of iterations per time step for the first 50 time steps for tolerances $\varepsilon = .1, .01, .001$, and .0001.

runs is $\varepsilon \leqslant .01$. Also shown for comparison in black is the same problem using the original difference formulation (*i.e.* $\overline{B} = B(t_0 + \Delta t)$). Overall there is good agreement between the methods; the main discrepancy occurs only at early times. The difference here can be attributed to the fact that during the first time step of a run using the explicit reference field of Eq. (21), the spatial gradient is much larger than in a fully implicit treatment, leading to higher energy flow. Since the original difference formulation is fully implicit, the smaller spatial gradient at the end of the time step leads to a lower energy flow. This is apparent during the first few time steps, as shown in Fig. 4, but the discrepancy evaporates once the problem has run for a while. Suitable time step control removes the discrepancy.

In Fig. 5 we show, at consecutive time steps, the number of iterations needed before our termination criterion is met for different values of ε. The time steps shown in Fig. 5 span the first 1/2 sh of the problem described in the previous paragraph. A remarkable feature born out in this figure is that, on average, the number of iterations for a given tolerance remains the same, even at early time steps when the Marshak wave is just penetrating the slab. For values of $\varepsilon \leqslant .01$, our solutions are visibly indistinguishable. We have made no attempts to accelerate the iteration process.

4.3. Thin/thick interface example

As already alluded to in the introduction, there are instances when the reference field used in the original difference formulation is a poor approximation for the actual radiation field, leading to noise induced crashes. We give a specific example of such a scenario in what follows.

4.3.1. Problem setup

In this example the slab length is .1 cm, has $\rho C_v = .3$ jerk/cm^3, has reflective boundary conditions applied to the left edge, and is open to vacuum on the right edge. There is an optically thin/thick interface at $x_b = .025$ cm, where to the left the gray opacity is $\sigma = .003$ cm^{-1}, and to the right is $\sigma = 300$ cm^{-1}. With our zoning, this corresponds to $\approx 5 \times 10^{-6}$ mean free paths per zone in the thin region, and ≈ 0.5 mean free paths per zone in the thick region. Initially the entire slab has a temperature of .05 keV, the difference field $D = I - B$ is zero, and there is a constant volumetric heat source in the optically thin region that heats the material there at .95 jerks/cm^3 sh. Because of the volumetric heat source, and the poor coupling to the radiation field in the optically thin region, the material temperature in the optically thin region rises at an almost constant rate.

4.3.2. Original difference formulation

For the original difference formulation, the reference field in the thin region corresponds to the material temperature there. Physically, however, the radiation temperature in the thin region is nowhere near the temperature of the material there because the coupling between the material and the radiation is weak; rather the radiation temperature in the thin region is almost equal to the material temperature at the surface of the thick region where emission and absorption are strong.

One expects the statistical fluctuations due to Monte Carlo transport to be large in the optically thin region, because the actual radiation field deviates significantly from a black body at the local material temperature there. Fig. 6 confirms this

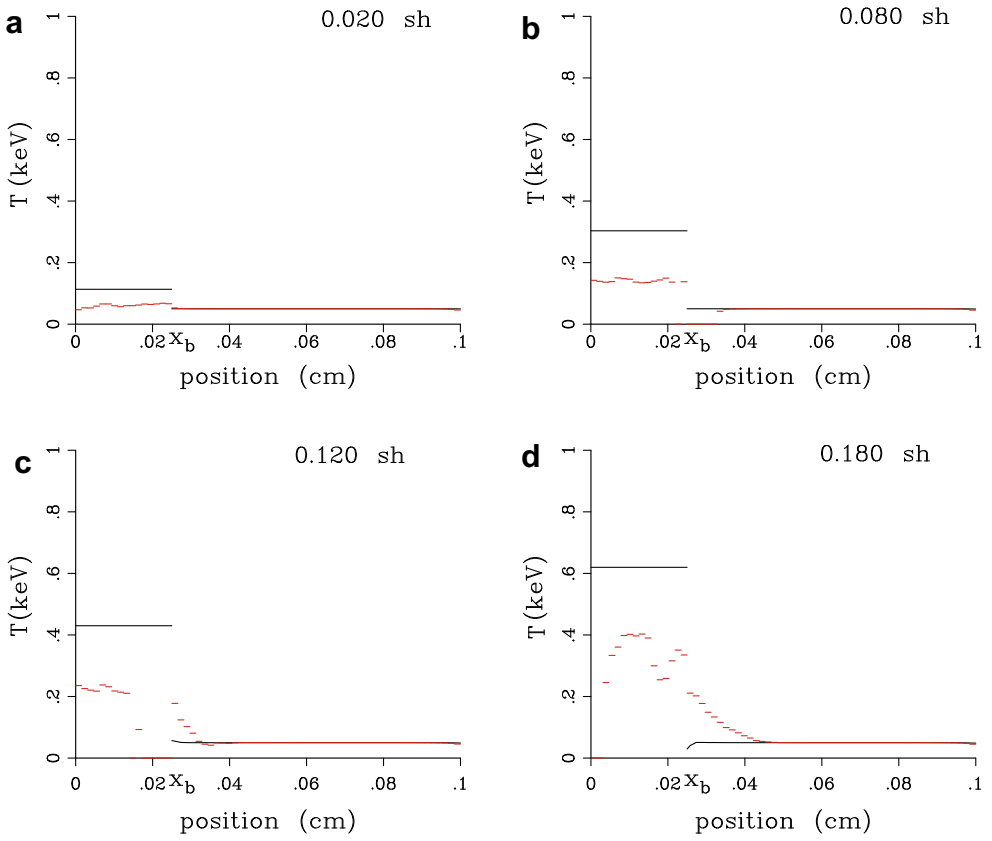

Fig. 6. Results showing radiation temperature as measured by the radiation energy density (red) and material temperature (black) when using the original difference formulation $\overline{B} = B(t)$ at various times. Note the large fluctuations in both radiation and material temperature as the difference in material temperature between the thick and thin regions increases.

expectation. The temperature of the radiation field as measured by its energy density, shown in red, fluctuates even at early times when the difference between the material temperatures of the thick and thin regions is relatively small. As this difference increases, fluctuations in the material temperature near the surface of the optically thick region, driven by fluctuations in the radiation energy density, become noticeable. For times larger than those shown in Fig. 6, these fluctuations lead to a code crash due to a negative material temperature. Note that in these plots, the floor temperature of the radiation field (as measured by its energy density, aT^4) is set to zero. Negative excursions of the radiation energy density are clipped in the figure, but they do occur.

4.3.3. Generalized reference field

Instead of using a reference field that corresponds to a black body derived from the material temperature in the optically thin region, we now choose $\overline{B}$ in the thin region to be that of the thick region just to the right of x_b, the position of the material interface.

$$\overline{B}(x,t) = \begin{cases} B(x_b, t_0) & \text{if } x < x_b, \;\; t_0 < t \leqslant (t_0 + \Delta t), \\ B(x, t_0) & \text{if } x \geqslant x_b, \;\; t_0 < t \leqslant (t_0 + \Delta t). \end{cases} \tag{38}$$

The arguments of $\overline{B}$ are made explicit in Eq. (38) to show its dependence on position, as well as time. This particular reference field imposes two slight modifications to the sources shown in Section 3. First, since the reference field is constant in space within the thin region, there are no space derivative sources emanating within this region. Second, since the reference field is continuous at the thin/thick interface, there is no delta function source at this interface.[3]

As Fig. 7 shows, statistical variations of the radiation temperature as measured by the radiation energy density (red), though still apparent, are much smaller than in Fig. 6. Furthermore, solutions to the material temperature (black) are stable. Indeed, with this choice of reference field, our code does not crash and can run indefinitely. Fig. 8 shows the radiation

[3] We could have chosen $\overline{B} = 0$ in the optically thin region, accepting additional noise in the solution once the optically thick surface at x_b heats up, and we would still avoid the problem crash at early time. Doing this might be expedient in more complicated problem geometries where choosing $\overline{B}$ could be difficult.

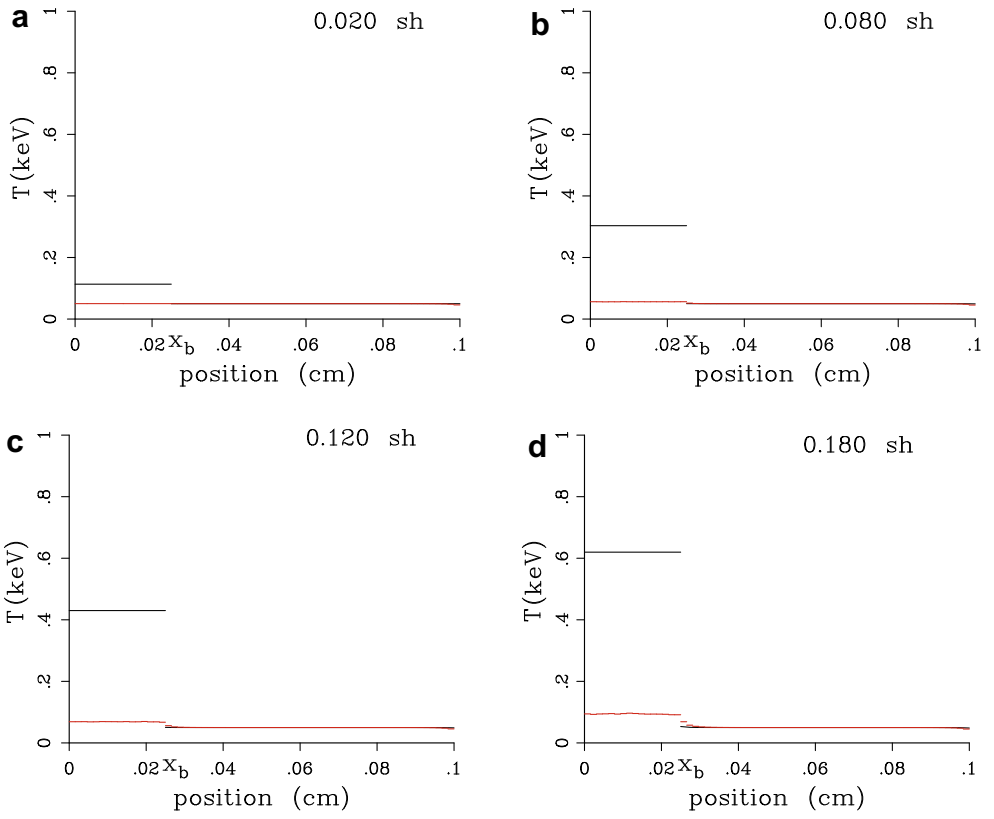

Fig. 7. Results showing radiation temperature (red) and material temperature (black) when using the reference field defined in Eq. (38) at various times. Note the relatively small fluctuations of the radiation temperature as compared to Fig. 6, as well as the stable material temperature profile of the slab near x_b.

temperature and material temperature after 800 time steps. Because of the constant volumetric heat source in the thin region, the material temperature here is 2.34 keV, well above the 1 keV range of the figure.

As seen from Figs. 7 and 8, the radiation temperature in the thin region is slightly higher than the material temperature of the thick region at the material interface x_b. This difference in radiation temperatures is what drives energy into the thick region. It is clear that the reference field defined in Eq. (38) is a good choice, as the difference field in the thin region is relatively small (but not zero).

Within the thick region the radiation temperature at the leading edge of the Marshak wave is at first larger than the material temperature. As the wave propagates, the temperatures relax to each other within a timescale t_{rel} intrinsic to the material, thus the radiation comes into equilibrium (locally) with the material. The relaxation time t_{rel} is given by [16]

$$t_{rel} = \frac{1}{\beta\sigma c}, \tag{39}$$

where

$$\beta = \frac{4aT^3}{\rho C_v}. \tag{40}$$

For the parameters used in this problem, $t_{rel} \sim .5$ sh, which is consistent with our results.

Since the material temperature is initially lower than the radiation temperature at the foot of the Marshak wave in the thick region, and thus 'lags' the radiation temperature, there persists a region of width δ where the two temperatures disagree, as shown in Fig. 8. We can estimate how the width of this region, δ, scales with opacity σ. This can be seen by first noting that δ can be approximated by [17]

$$\delta \sim t_{rel} v_{mw}, \tag{41}$$

where v_{mw} represents the velocity of the Marshak wave [16]

$$v_{mw}(t) \sim \frac{1}{2}\sqrt{\frac{\kappa}{\rho C_v t}}. \tag{42}$$

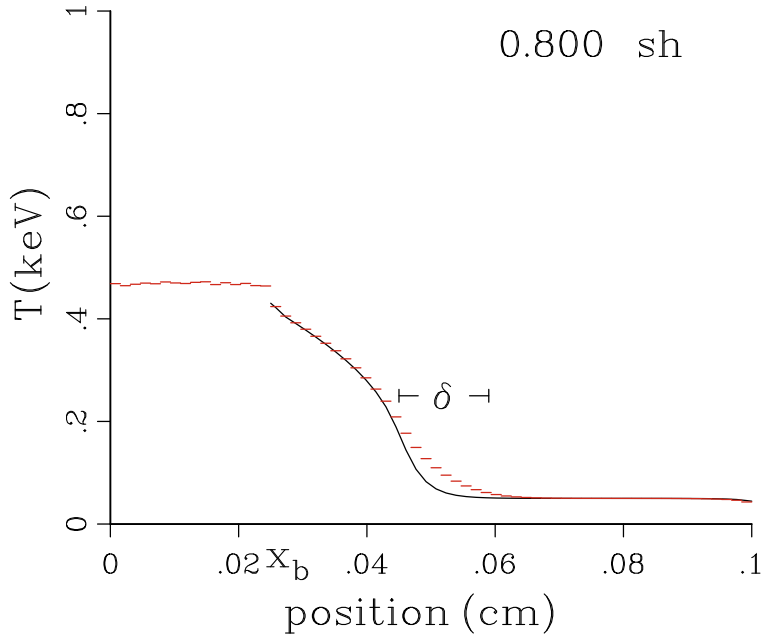

Fig. 8. The same problem as Fig. 7, but after many time steps. Note that due to the constant volumetric source in the thin region, the material temperature in this region is 2.34 keV, well above the range of the figure. Also note the temperature difference between the radiation field and material in the region labeled by δ in the thick region.

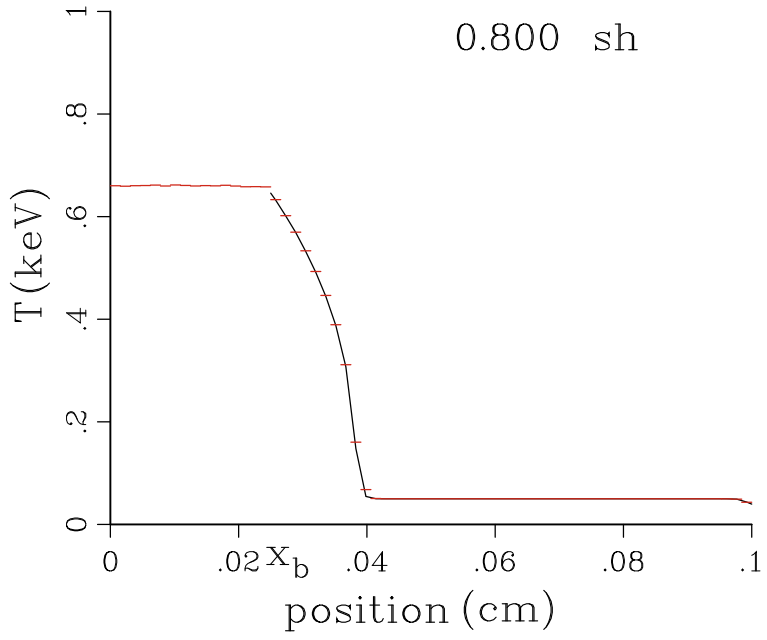

Fig. 9. Problem identical to that of Fig. 8, except that the opacity in the thick region has been increased by an order of magnitude (see text).

For gray opacities, the coefficient of radiative heat conduction, κ, is given by

$$\kappa \approx \frac{4ca}{3\sigma} T^3. \tag{43}$$

Combining these expressions gives

$$\delta \sim \frac{1}{\sqrt{12\beta}\sqrt{ct}\sigma^{3/2}}, \tag{44}$$

which shows that δ scales as $\sigma^{-3/2}$. This suggests that as the medium becomes thicker, the gap decreases (as expected). Fig. 9 qualitatively supports this statement, where a calculation analogous to the one presented in Fig. 8 is shown, but the opacity in the thick region is increased by an order of magnitude ($\sigma = 3000\ \mathrm{cm}^{-1}$). The gap in this case is too small to be seen in the figure.

5. Stability analysis

The overwhelming importance of unconditional stability demands that calculations in the standard formulation for transport, Eqs. (1) and (2), be done implicitly in time. For Monte Carlo implementations, the required implicit differencing is achieved using the Implicit Monte Carlo (IMC) method [5], or with the Symbolic Implicit Monte Carlo (SIMC) method [6], as the case may be. It is important to explore the stability requirements for the difference formulation.

When using the beginning of time step temperature, Eq. (21), to define the reference field for the difference formulation, the space derivative source term is evaluated explicitly and there is a concern that the resulting method might have a problem with stability. To address this we have conducted a detailed stability analysis. We provide a synopsis of the stability analysis in this section, reporting relevant results. Readers interested in the details of the analysis can find them in [9].

We restrict our analysis to optically thick zones and slab geometry. We also assume that there are no energy sources or sinks and that the system is close to equilibrium, in a diffusive regime. We give now qualitative arguments that these conditions are the most unstable ones. Consider an interface between two optically thick zones and assume that there is a small temperature difference between them. We will call the hotter one zone 1 and the colder one zone 2. The difference in temperature causes a flux of radiation to flow from zone 1 to zone 2. When the zones are optically thick, the flow does not depend on the conditions of the other zones since all photons that are emitted in one of the zones – and penetrate into the other zone – are absorbed there. Let us consider what happens in one time step. In reality, the temperature difference diminishes and so does the flux. In our discretization schemes the conditions in each zone are constant during the time step, so radiation flows at a steady rate. If the time step is long enough, and the heat capacity of zones 1 and 2 are small enough, zone 2 can get hotter than zone 1, so the temperature difference becomes oscillatory. The absolute temperature difference may even increase in a time step: this is the cause of numerical instability.

Our experience with the Monte Carlo code implementations discussed in this paper, consistent with the description above, is that short wavelength instabilities dominate. We perform our analysis in the optically thick limit, employing a two zone problem with periodic boundary conditions, expecting that we can capture the behavior we observe. Initial conditions are shown in Fig. 10. The initial difference field is zero. It is useful to write $\Phi_1 = \Phi_0 + \Delta\Phi_1$ and $\Phi_2 = \Phi_0 + \Delta\Phi_2$, as we are interested in small perturbations, $|\Delta\Phi_i| \ll \Phi_0$, with the optically thick limit providing the constraints $1/\sigma\Delta x \ll 1$ and $1/\sigma c\Delta t \ll 1$. These constraints allow for a simplified, but by no means simple, derivation of the sources and their contributions to the energy balance of the zones. The periodic boundary conditions imply that all particles that exit to the right of $x = 2\Delta x$ immediately enter at $x = 0$, and vice versa for particles exiting to the left of $x = 0$.

The synopsis of the stability analysis, for each case we consider, is as follows. For each source term appearing in the transport equation, we calculate its energy deposition in the zone in which the particles were born, as well as in the adjacent zone. Because we are in the thick limit, photons do not propagate further than the zone adjacent to the one they were born in and this possibility is neglected. Energy depositions due to the source terms and holdover energy (the photons still in flight at the end of the time step) are calculated, dropping terms containing higher orders in $1/\sigma\Delta x$ and $1/\sigma c\Delta t$, when appropriate, to simplify the analysis. Given the energy depositions from the source terms, the energy equation can be solved for $\Delta\Phi_i(t_0 + \Delta t)$ in terms of $\Delta\Phi_i(t_0)$ and then their ratio can be considered.

Stability is obtained if

$$\left|\frac{\Delta\Phi_i(t_0 + \Delta t)}{\Delta\Phi_i(t_0)}\right| < 1, \tag{45}$$

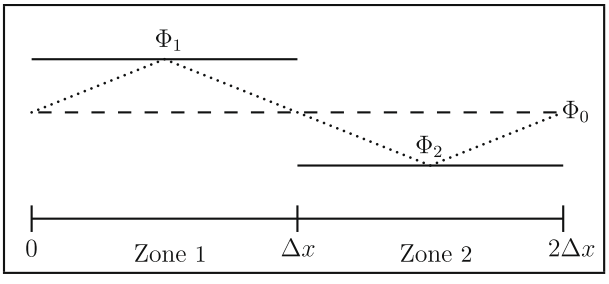

Fig. 10. Initial conditions for performing the stability analysis. Periodic boundary conditions are used, photons that exit the problem at $x = 2\Delta x$ re-enter at $x = 0$, and vice versa. The dotted line is the interpolation of Φ between zone centers that is used for the space derivative source term, the other source terms use the constant representation of Φ within a zone. The dashed line at Φ_0 is the equilibrium energy density. The deviations from it are small. There is no initial difference field.

assuring that the perturbation shrinks with time. The above constraint does not imply monotonic temporal behavior. This occurs only if

$$0 \leqslant \frac{\Delta\Phi_i(t_0+\Delta t)}{\Delta\Phi_i(t_0)} < 1. \tag{46}$$

To minimize clutter we introduce the following notation:

$$\varepsilon_x \equiv \frac{1}{\sigma\Delta x}, \tag{47}$$

$$\varepsilon_t \equiv \frac{1}{\sigma\Delta t c},$$

$$\gamma \equiv \frac{c\Delta t}{\Delta x}. \tag{48}$$

Thus the assumptions that $1/\sigma\Delta x \ll 1$ and $1/\sigma c\Delta t \ll 1$ are equivalent to $\varepsilon_x \ll 1$ and $\varepsilon_t \ll 1$, respectively.

It also useful to define

$$\beta_0 = 4aT_0^3/\rho C_v, \tag{49}$$

the ratio of specific heats for radiation and material in equilibrium at the same temperature, T_0.

With our approach to the stability analysis laid out, we now move on to describing the results.

5.1. Original difference formulation using $\overline{B} = B(t_0 + \Delta t)$

The ratio for this choice of reference field is

$$\frac{\Delta\Phi_i(t_0+\Delta t)}{\Delta\Phi_i(t_0)} = \frac{1+\beta_0\left[1-\varepsilon_x-\frac{4}{3}\gamma\varepsilon_t\varepsilon_x\right]}{1+\beta_0\left(1-\varepsilon_x+\frac{4}{3}\gamma\varepsilon_x(1-2\varepsilon_t)\right)}, \tag{50}$$

the detailed calculations for which can be found in [9]. Given that β_0 is positive and that ε_t and ε_x are small positive quantities, the ratio is positive and less than one. The method is therefore unconditionally stable and monotonic in time. This supports, formally, the behavior that we have observed in practice for a wide range of problem parameters.

5.2. Generalized reference field using $\overline{B} = B(t_0)$

In this case the time derivative source produces a dependence on $\Delta\Phi_i(t_0 - \Delta t)$, leading to a recursion relation that connects three successive values of $\Delta\Phi$. A quadratic is produced that must be solved to find the ratio

$$\alpha = \frac{\Delta\Phi_i(t_0+\Delta t)}{\Delta\Phi_i(t_0)}. \tag{51}$$

There are two modes for the solutions to the recursion relation, each with its own growth rate, α. Expanding to order ε_x, the two values for α are given by

$$\alpha = \begin{cases} 1-\varepsilon_x\frac{4}{3}\frac{\beta_0\gamma}{1+\beta_0(2+\gamma)} + O\left(\varepsilon_x^2, \varepsilon_x\varepsilon_t\right), \\ \varepsilon_x\frac{\beta_0}{1+\beta_0(1+\gamma)} + O\left(\varepsilon_x^2, \varepsilon_x\varepsilon_t\right). \end{cases} \tag{52}$$

A general solution to the recurrence relation will involve a linear combination of both modes with the most rapidly growing one controlling whether or not the method is stable. Fortunately, α is positive and less than 1 for both modes, indicating that the method is unconditionally stable and monotonic in time.

5.3. Taylor expansion of $\sigma(B - \overline{B})$

When employing $\overline{B} = B(t_0)$ as the reference field, only the remainder source term contains a dependence on the unknown $B(t_0 + \Delta t)$, and therefore $\Phi(t_0 + \Delta t)$. It is this dependence upon the unknown end of time step value of Φ that leads to symbolic scoring of Monte Carlo particles and the requirement for the solution of a non-linear system at the end of the time step.

For a sufficiently small time step, one might approximate the remainder source term by

$$\sigma(B(t_0+\Delta t) - B(t_0)) \approx \sigma\Delta B = \sigma\Delta t\frac{\partial B(t)}{\partial t}, \tag{53}$$

where the time derivative is evaluated explicitly using the values from the previous time step. If the resulting scheme is stable, it would be preferred as it would remove the costs associated with solving a non-linear system in order to produce the end of time step temperatures.

In this case, our stability analysis again leads to a recursion relation connecting three successive values of $\Delta\Phi$. We expand the solutions for α, the growth rates, to first order in ϵ_x, obtaining

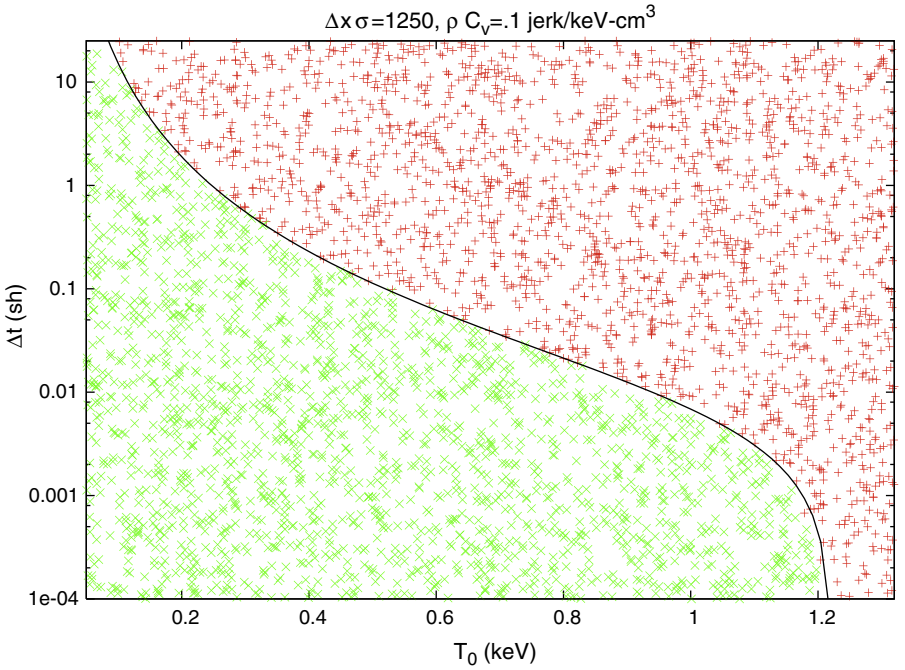

Fig. 11. Scatter plot showing numerical results that demarcate stable, green, and unstable, red, runs. The solid black line is the derived stability criterion given by Eq. (55). The zone size, Δx, is 2.5 cm.

$$\alpha = \begin{cases} 1 - \varepsilon_x \frac{4}{3} \frac{\beta_0 \gamma}{1+\beta_0(1+\gamma)} + O(\varepsilon_x^2, \varepsilon_x \varepsilon_t), \\ -\beta_0(1+\gamma) + \varepsilon_x \frac{\beta_0(6-2\beta_0(\gamma(1+4\gamma)-3)}{6(1+\beta_0(1+\gamma))} + O(\varepsilon_x^2, \varepsilon_x \varepsilon_t). \end{cases} \tag{54}$$

One of the modes is unstable when

$$\beta_0(1+\gamma) > 1,$$

or, equivalently, when

$$\gamma = \frac{c\Delta t}{\Delta x} > \left(\frac{1}{\beta_0} - 1\right). \tag{55}$$

In Fig. 11, we plot $\Delta t = \Delta x(\beta_0^{-1} - 1)/c$ (the black line) for the particular parameters labeled in the figure. Runs with randomly sampled initial temperatures, T_0, and time step sizes, Δt, were performed with initial conditions shown in Fig. 10. Stability was determined by examining the growth, or shrinkage, of an initial perturbation in Φ for a two zone problem with periodic boundary conditions. Runs that were stable are plotted in green, whereas unstable runs are shown in red. Note that the demarcation between stable and unstable is well predicted by the black line.

A closer look at our definition for β, Eq. (49), shows that unavoidable stability trouble sets in as the "specific heat" for the radiation field matches that of the material, forcing the time step to zero. An explicit treatment of the remainder source term is not very useful, but the good match between the stability analysis and the numerical results convinces us of the correctness of our analysis for those cases where unconditional stability is predicted.

6. Conclusion

In this paper, we have evaluated generalizations of the difference formulation that use reference fields other than the black body corresponding to the implicitly differenced local material temperature. We have shown that by using the black body corresponding to the material temperature at the beginning of the time step, the remainder of the thermal emission term is small when the problem is slowly varying. This provides a material energy equation that is amenable to an efficient iterative solution and addresses the cost associated with the Newton–Raphson solve that is required in the original difference formulation.

In problems with optically thin regions adjacent to optically thick ones, cancellation of the space derivative source terms can cause high levels of noise with attendant problem crashes. To resolve this problem we have explored using the black

body corresponding to the temperature of the adjacent optically thick region for the reference field in the optically thin region, finding that it removes the noise induced problem crashes.

The SIMC method is more sensitive to the problem of excess energy flow in the thick limit, compared to the IMC method, because the energy of the radiation field is correctly coupled to the material energy. The full machinery of the linear discontinuous finite element method [3,4] can be used to address excess energy flow, but we have found an ad-hoc interpolation scheme that produces the correct flux between zones in the thick limit without resorting to the more costly finite element method. We have demonstrated this interpolation scheme for problems in 1D slab geometry and will investigate extending it to higher dimensions in a future work.

In addition to our numerical results which are of practical importance, we have explored the stability of the difference formulation in the optically thick limit. We find the difference formulation to be unconditionally stable, regardless of the choice of reference field, as long as source terms that depend on the unknown end of time step temperature are treated implicitly.

References

[1] A. Szoke, E. Brooks III, The transport equation in optically thick media, J. Quant. Spectrosc. Radiat. Transfer 91 (2005) 95.
[2] E. Brooks III, M. McKinley, F. Daffin, A. Szoke, Symbolic implicit Monte Carlo radiation transport in the difference formulation: a piecewise constant discretization, J. Comput. Phys. 205 (2005) 737–754.
[3] J.-F. Clouet, G. Samba, Asymptotic diffusion limit of the symbolic Monte-Carlo method for the transport equation, J. Comput. Phys. 195 (2004) 293.
[4] E. Brooks III, A. Szoke, J. Peterson, Piecewise linear discretization of symbolic implicit Monte Carlo radiation transport in the difference formulation, J. Comput. Phys. 220 (2006) 471–497.
[5] J. Fleck, J. Cummings, An implicit Monte Carlo scheme for calculating time and frequency dependent radiation transport, J. Comput. Phys. 8 (1971) 313.
[6] E. D Brooks III, Symbolic implicit Monte Carlo, J. Comput. Phys. 82 (1986) 433–446.
[7] T. N'kaoua, Solution of the nonlinear radiative transfer equations by a fully implicit matrix Monte Carlo method coupled with the Rosseland diffusion equation via domain decomposition, SIAM J. Sci. Stat. Comput. 12 (1991) 505.
[8] J. Densmore, E. Larsen, Asymptotic equilibrium diffusion analysis of time-dependent Monte Carlo methods for grey radiative transfer, J. Comput. Phys. 199 (2004) 175–204.
[9] T.C. Luu, E.D. Brooks III, A. Szoke, Generalized subtraction schemes for the difference formulation in radiation transport, Lawrence Livermore National Laboratory, LLNL-TR-408299, 2008. <http://library-ext.llnl.gov>.
[10] J.I. Castor, Radiation Hydrodynamics, Cambridge University Press, 2004.
[11] T.C. Luu, E.D. Brooks III, A. Szoke, Source tilting within the difference formulation for radiation transport, Lawrence Livermore National Laboratory, UCRL-JRNL-225197, 2006. <http://library-ext.llnl.gov>.
[12] R.P. Smedley-Stevenson, Improved implicit Monte Carlo schemes based on the difference formulation, in: Joint International Topical Meeting on Mathematics and Computation and Supercomputing in Nuclear Applications (M&C + SNA 2007), Monterey, California, April 15–19, 2007, on CD-ROM, American Nuclear Society, LaGrange Park, IL, 2007.
[14] E. Larsen, A grey transport acceleration method for time-dependent radiative transfer problems, J. Comput. Phys. 78 (1987) 459.
[15] B. Chang, The incorporation of the semi-implicit linear equations into Newton's method for solving radiative transfer equations, J. Comput. Phys. 226 (2007) 852–878.
[16] Y.B. Zel'dovich, Y.P. Raizer, Physics of Shock Waves and High-temperature Hydrodynamic Phenomena, Dover Publications, 1966.
[17] D. Mihalas, B. Weibel-Mihalas, Foundations of Radiation Hydrodynamics, Dover Publications, 1984.